Estimating the Propagation Velocity Distribution and the Position of Buried Pipes Using $x-t-v$ Data Matrix of Subsurface Radar Image

Yasuhiro FUJIMURA[†] and Akira KAWANAKA [†]

Faculty of Science and Technology, Sophia University

Hideki HAYAKAWA [‡]

Fundamental Research Laboratories, OSAKA GAS Co.,Ltd.

Abstract

We propose a new method of radar imaging of underground pipes in inhomogeneous soil, which does not require a priori knowledge of the propagation velocity of electromagnetic waves in soil. In this method, three-dimensional $x-t-v$ data matrix from multiple migrated radar images with different propagation velocities using F-K migration method is composed. And we extract the hyperbolic apex and estimate the propagation velocity of each hyperbola, using the $x-t-v$ data matrix. By interpolating these estimated discrete propagation velocities along the t-axis, the propagation velocity distribution downward in the soil is derived. The reconstructed image of the underground section in inhomogeneous soil is obtained by extracting the image intensity from the $x-t-v$ data matrix based on the derived propagation velocity distribution. Furthermore the influences by thick buried pipes are considered, and the diameter estimation method is described. The effectiveness of new method is demonstrated by comparison with previous methods. The new method accurately reconstructs the underground section in inhomogeneous soil at low computing cost.

1 Introduction

The techniques for imaging optically opaque region using an electromagnetic wave radar are being developed. One important application of these techniques is an imaging of underground objects such as buried pipes and cables. The image quality of subsurface radar often becomes poor since the electromagnetic wave is attenuated seriously in soil and is affected by its inhomogeneity.

To improve signal-to-noise ratio and resolution of the radar images, the aperture synthesis method or the migration method are generally applied. These methods require a priori knowledge of electromagnetic wave propagation velocity. In addition, since propagation velocity of the electromagnetic wave affects the accuracy of buried object depth, it is important to estimate the propagation velocity.

Tsuchihashi et al. (1989) proposed a method of velocity estimation using aperture synthesis radar images with different propagation velocities[1]. This method assumes that the propagation velocity is uniform over the subsurface section. Including the case of inhomogeneous soil, Osumi and Ueno (1985) proposed the holographic imaging method based on the geometric shape of the hyperbolic curve[2]. However, the holographic imaging method requires the solution of a nonlinear optimization problem at each pixel over the radar image, with computational inefficiency. Stolte and Nick (1994) proposed the eccentricity-migration method, which automatically determines the diameters of buried pipes without a priori knowledge of electromagnetic wave propagation velocity[3]. However, this method involves considerable computational expense, since it calculates the summed-up energy along many kinds of hyperbolic curves over the radar image. Furthermore, this method is not sufficient to improve the radar image resolution when two buried pipes are close together.

To solve the problems of these methods, we propose a new method of radar imaging of underground pipes in inhomogeneous soil, without a priori knowledge of the propagation velocity.

First, the $x-t$ radar image is processed by the migration in wavenumber-frequency domain for various propagation velocities v. These multiple migrated images are then stacked in the direction of the v-axis in the $x-t-v$ data matrix. We can simultaneously extract the hyperbolic apex and estimate the propagation velocity of each hyperbola, using the $x-t-v$ data matrix. Next, interpolating these estimated discrete propagation velocities along the t-axis, we can derive the propagation velocity distribution $v(t)$ downward in the soil. Finally, we yield a reconstructed image of the underground section in inhomogeneous soil with the derived propagation ve-

[†]Address: 7-1 Kioi-cho, Chiyoda-ku, Tokyo 102, Japan. E-mail: yasu@akira.ee.sophia.ac.jp

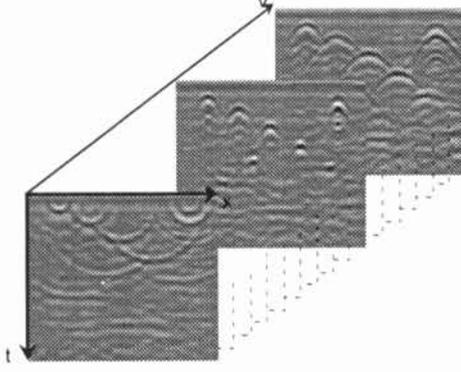[‡]Address: 6-19-9 Torishima, Konohana-ku, Osaka 554, Japan.

Figure 1: Multiple migrated images with various propagation velocity v_k are stacked in the direction of the $v-$axis in the $x-t-v$ data matrix $f(x_i, t_j, v_k)$.

locity distribution $v(t)$.

The new method is based on the supposition that the diameter of each buried pipe is negligible to its depth from the ground surface. The influence to the estimation values by thick pipes is considered and the estimation method of their diameters is described.

2 $X-T-V$ Data Matrix Operation

2.1 $X-T-V$ Data Matrix Formulation

The image intensity $f(x_i, t_j)$, obtained using the subsurface radar system, is processed by the migration in wavenumber-frequency domain for various propagation velocities v_k (Stolt, 1978)[4]. Here, $i = 1, 2, \cdots, l$, $j = 1, 2, \cdots, n$. These multiple migrated images are then stacked in the direction of the $v-$axis in the $x-t-v$ data matrix $\hat{f}(x_i, t_j, v_k)$, shown in Fig. 1.

2.2 Extraction for Hyperbolic Apex and Velocity Estimation

The reflected signal of a point reflector such as thin buried pipe shapes a hyperbolic curve in the radar image. As well, the reflected signal of the point reflector at a certain depth focuses at the hyperbolic apex, when velocity v_k coincides with the mean propagation velocity between the ground surface and the depth of the hyperbolic apex.[1] Since the intensity at the hyperbolic apex shows a sharp peak in the direction of the $v-$axis in the $x-t-v$ data matrix $\hat{f}(x_i, t_j, v_k)$, the (x_i, t_j) points at which intensity shows sharp peak along the $v-$axis are detected as candidates for propagation velocity estimation points.

---

[1]Hereafter, the mean propagation velocity is simply called the propagation velocity.

To be more concrete, average intensity $ave(x_i, t_j)$, peak intensity $p(x_i, t_j)$ and peak value $pv(x_i, t_j)$ at each (x_i, t_j) point are calculated as:[2]

$$ave(x_i, t_j) = \frac{1}{n} \sum_{k=1}^{n} \hat{f}(x_i, t_j, v_k) \qquad (1)$$

$$p(x_i, t_j) = \begin{cases} \max_{1 \leq k \leq n} \hat{f}(x_i, t_j, v_k) \\ \qquad\qquad \text{if} \quad ave(x_i, t_j) \geq 0 \\ -\min_{1 \leq k \leq n} \hat{f}(x_i, t_j, v_k) \\ \qquad\qquad \text{if} \quad ave(x_i, t_j) < 0 \end{cases} \qquad (2)$$

$$pv(x_i, t_j) = \begin{cases} p(x_i, t_j) - \max\{ave(x_i, t_j), \\ \qquad \hat{f}(x_i, t_j, v_1), \hat{f}(x_i, t_j, v_n)\} \\ \qquad\qquad \text{if} \quad ave(x_i, t_j) \geq 0 \\ p(x_i, t_j) + \min\{ave(x_i, t_j), \\ \qquad \hat{f}(x_i, t_j, v_1), \hat{f}(x_i, t_j, v_n)\} \\ \qquad\qquad \text{if} \quad ave(x_i, t_j) < 0 \end{cases} \qquad (3)$$

The (x_i, t_j) points at which peak value $pv(x_i, t_j)$ is larger than threshold T_1 are extracted, and interconnected regions are obtained. In each region, the (x_i, t_j) points at which peak intensity $p(x_i, t_j)$ is maximum are extracted. We call these extracted points candidates for propagation velocity estimation points $(\tilde{x}_s, \tilde{t}_s)$. Here, subscript s is the number of candidates for propagation velocity estimation points. The propagation velocity of each point $(\tilde{x}_s, \tilde{t}_s)$ is determined by the peak intensity point's velocity $v_p(\tilde{x}_s, \tilde{t}_s)$ along the $v-$axis in the $x-t-v$ data matrix.

2.3 Error Rejection

In the well-migrated radar image, the reflected signal of the point reflector focuses at the hyperbolic apex. This characteristic phenomena is therefore used to eliminate erroneous candidates for propagation velocity estimation points.

First, the binary images $\hat{f}_{\text{bin}}(x_i, t_j, v_k)|_{v_k = v_p(\tilde{x}_s, \tilde{t}_s)}$ are obtained from each migrated image $\hat{f}(x_i, t_j, v_k)|_{v_k = v_p(\tilde{x}_s, \tilde{t}_s)}$ with the propagation velocity $v_p(\tilde{x}_s, \tilde{t}_s)$ of each candidate point $(\tilde{x}_s, \tilde{t}_s)$ as:

$$\hat{f}_{\text{bin}}(x_i, t_j, v_k)|_{v_k = v_p(\tilde{x}_s, \tilde{t}_s)}$$

$$= \begin{cases} 1 & \text{if} \quad \left| \hat{f}(x_i, t_j, v_k)|_{v_k = v_p(\tilde{x}_s, \tilde{t}_s)} \right| \\ & \qquad\qquad \geq p(\tilde{x}_s, \tilde{t}_s) - T_1 \\ 0 & \text{if} \quad \left| \hat{f}(x_i, t_j, v_k)|_{v_k = v_p(\tilde{x}_s, \tilde{t}_s)} \right| \\ & \qquad\qquad < p(\tilde{x}_s, \tilde{t}_s) - T_1 \end{cases} \qquad (4)$$

Next, in the obtained binary image $\hat{f}_{\text{bin}}(x_i, t_j, v_k)|_{v_k = v_p(\tilde{x}_s, \tilde{t}_s)}$, the area value of interconnecting regions with $(\tilde{x}_s, \tilde{t}_s)$ is calculated. The normalized area value is then obtained by dividing the

---

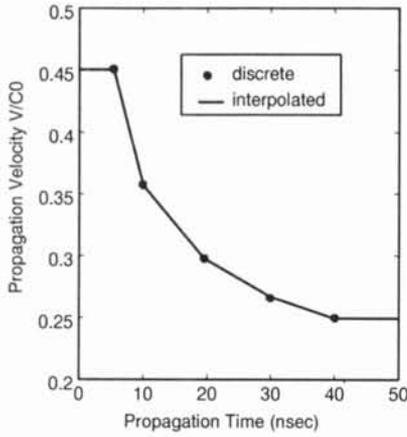[2]The peak value is defined by the difference value between the peak and the average intensity.

Figure 2: Sample of the velocity distribution $v(t)$ calculated by the linear interpolation of discrete velocity values $v_p(\hat{x}_t, \hat{t}_t)$. The points represent the discrete velocity values $v_p(\hat{x}_t, \hat{t}_t)$; the solid line represents the interpolated velocity distribution $v(t)$.
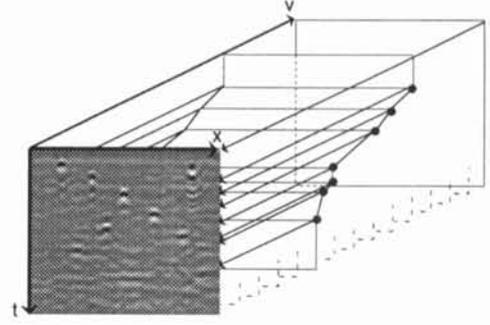

Figure 3: Extraction of the image intensity form the $x-t-v$ data matrix along with the derived propagation velocity distribution $v(t)$, yielding a reconstructed image of underground section in inhomogeneous soil.

area value by the peak value $pv(\tilde{x}_s, \tilde{t}_s)$. The candidate points $(\tilde{x}_s, \tilde{t}_s)$, whose normalized area values are smaller than threshold value T_2, are then selected.

Antenna of subsurface radar causes ringing phenomena with constant interval along the t–axis, because the energy in the impulse wave form near zero Hertz is not radiated by the antenna. Based on the ringing phenomena, the candidate point is grouped with the near candidate points and only those points are extracted. Here, the constant interval corresponds to the transmitted pulse width, it is determined by the antenna bandwidth and a carrier frequency equal to the antenna center frequency.

In each set of extracted points, the point at which $|p(\tilde{x}_s, \tilde{t}_s)|$ is maximum is selected as the propagation velocity estimation point $(\hat{x}_t, \hat{t}_t)$. Here, subscript t is the number of extracted point sets and corresponds to the number of propagation velocity estimation points. Of course, the propagation velocity of each point $(\hat{x}_t, \hat{t}_t)$ corresponds to the peak intensity point's velocity $v_p(\hat{x}_t, \hat{t}_t)$ along the v–axis in the $x-t-v$ data matrix.

2.4 Velocity Interpolation and Image Reconstruction

Electromagnetic wave propagation velocity depends on the moisture of the soil, which often varies with depth from the surface. We therefore assume the propagation velocity to be variable depending on depth, and estimate propagation velocity distribution $v(t)$ in the depth direction (Ho and Kawanaka, 1995)[5]. First, propagation velocity of estimation points $v_p(\hat{x}_t, \hat{t}_t)$ are projected onto the t–axis. Then, the propagation velocity distribution $v(t)$ is obtained by linear interpolation of discrete

velocity values $v_p(\hat{x}_t, \hat{t}_t)$ as shown in Fig. 2.

To derive a more correct propagation velocity distribution $v(t)$, we impose the constraint that the order of the reflected depth corresponds to the order of one-way propagation time. In other words, if propagation time t is shorter, the depth must be shallower. If propagation velocity estimation point $(\hat{x}_t, \hat{t}_t)$ satisfies $\hat{t}_t \cdot v_p(\hat{x}_t, \hat{t}_t) < (\hat{t}_t - \Delta t) \cdot v(\hat{t}_t - \Delta t)$, the propagation velocity estimation point is eliminated. The propagation distribution $v(t)$ is then recalculated by linear interpolation. The above order check of the reflected depth and velocity interpolation is repeated until no propagation velocity estimation point is eliminated.

Finally, as shown in Fig. 3, the image intensity is extracted from the $x-t-v$ data matrix along with the derived propagation velocity distribution $v(t)$, yielding a reconstructed image of underground section in inhomogeneous soil. The depth scale of the reconstructed image $d(t)$ can be determined by the derived propagation velocity distribution $v(t)$ and one-way propagation time t.

$$d(t_j) = t_j \cdot v(t_j) \qquad j = 1, 2, \cdots, m \qquad (5)$$

3 Experiments

3.1 Image Processing with $x-t-v$ Data Matrix

The subsurface radar image and its cross-section are shown in Fig. 4. This image obtained by impulse-radar of center frequency about 400 MHz, is preprocessed by the time calibration for zero-offset and auto gain control in the direction of the time axis. The sampling intervals of this radar system are $\Delta t = 0.28$ns and $\Delta x = 2.5 \times 10^{-2}$m. Image size is 200×171 pixels and resolution is 8bit/pixel. The upper side of the image represents the ground surface.
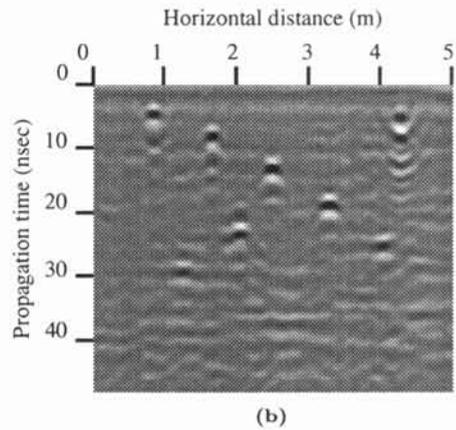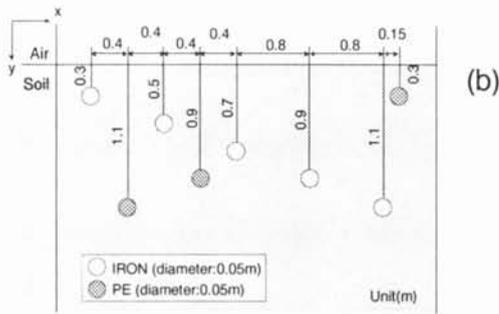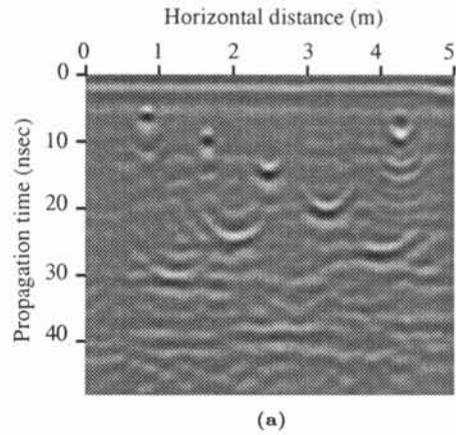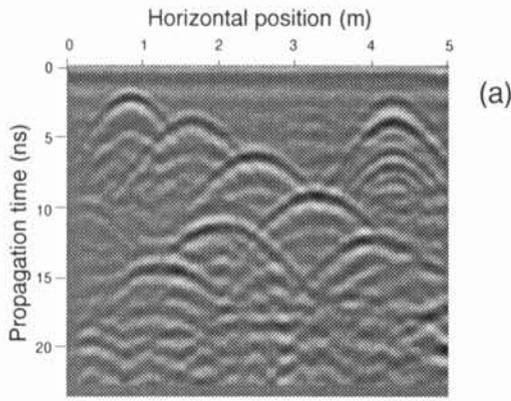
Figure 4: Subsurface radar image and its cross-seciton. (a) subsurface radar image obtained by impulse-radar; (b) cross-section.

The vertical direction represents one-way propagation time. The hyperbolic shapes correspond to the buried pipes. In this image there are five iron pipes and three polyethylene pipes.

First, we use a method of propagation velocity estimation assuming that the measurement region is homogeneous. The reconstructed image obtained by the homogeneous assumption method is shown in Fig. 5(a).

We then use our proposed $x-t-v$ data matrix method. The estimated velocity distribution is shown in Fig. 6. Then, the reconstructed image obtained using this propagation velocity distribution is shown in Fig. 5(b). All the hyperbolic reflected images of the buried pipes are converged, and the reconstructed images are improved, to yield the correct locations of the buried pipes. The horizontal resolution of the image reconstructed using the $x-t-v$ data matrix method is better than that using the simple multiple migration method.

3.2 Influence of Thick Buried Pipe

The propagation velocity distribution can be estimated using the migration method with assumption that the diameter of buried pipe is negligible comparing with its depth. The existence of thick buried pipe in the measurement area affects the estimated propagation velocity. As such a case, another radar

Figure 5: Images reconstructed by three methods. (a) homogeneous assumption method; (b) $x-t-v$ data matrix method.
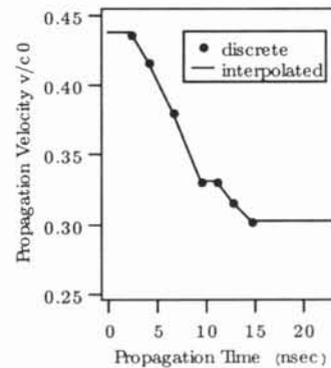

Figure 6: Estimated propagation velocity distribution $v(t)$.

image is shown in Fig. 7. This image obtained by impulse-radar of center frequency about 360 MHz. The sampling intervals of this radar system are $\Delta t = 0.41$ns and $\Delta x = 2.5 \times 10^{-2}$m. In this image there are four pipes at almost equal depth. And from the left, first (pipe 1) and third one (pipe 3) have diameters of smaller than 35 [mm], while second one (pipe 2) has diameter of 300 [mm] and forth (pipe 4) has 400 [mm].

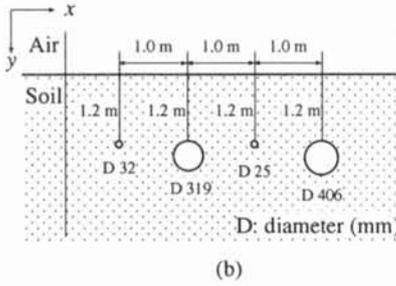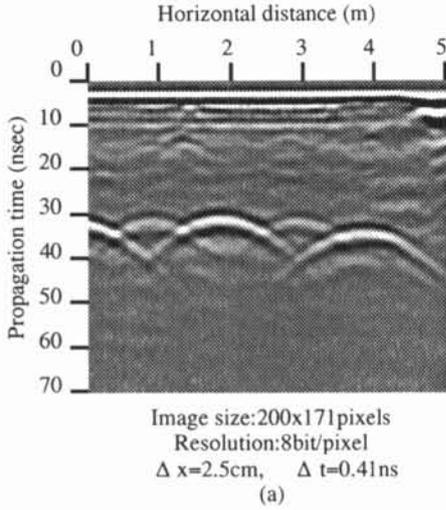Image size:200x171pixels
Resolution:8bit/pixel
Δ x=2.5cm, Δ t=0.41ns
(a)

D: diameter (mm)

(b)

Figure 7: Subsurface radar image containing thick pipes, and its cross-seciton. (a) subsurface radar image; (b) cross-section.
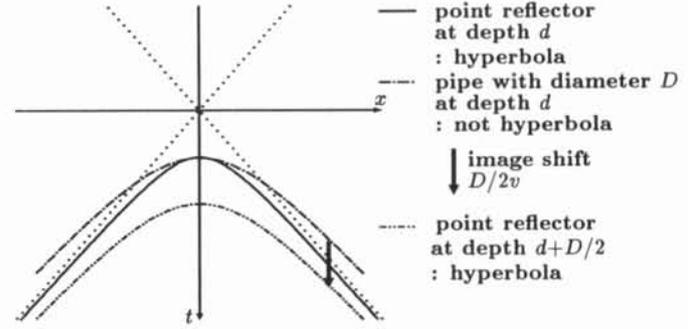

Figure 8: Radar image shifted along t-axis. If the radar image from a buried pipe with diameter D is shifted downward by $D/2v$, the reflection shapes a strict hyperbola.
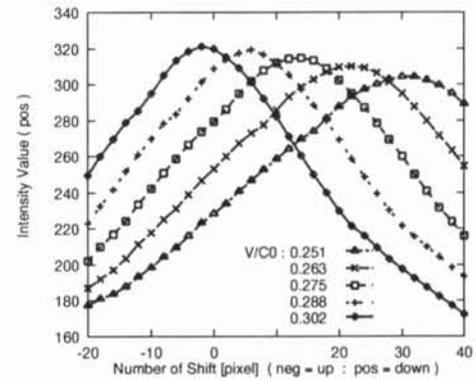

Figure 9: Migrated intensity value of pipe 2 (second pipe from left side) in Fig. 7 when the image shift is changed.

Table 1: Estimated propagation velocity and depth for Fig. 7 using the x-t-v data matrix method.

	pipe 1	pipe 2	pipe 3	pipe 4
Estimated propagation velocity V/C_0	0.275	0.302	0.275	0.288
Estimated depth [m]	1.19	1.28	1.19	1.35

The estimated propagation velocity from four pipes of this image by using the x-t-v method is shown in Table. 1. If propagation velocity depends on depth from the surface, the estimated propagation velocity from four pipes at almost same depth has to be equal. However, in Table. 1, the estimated propagation velocities from four pipes show different values each other. It is thought that the diameters of pipe 1 and pipe 3 are negligible comparing with their depth, but those of pipe 2 and pipe 4 affect the estimated values. So an estimation method of the diameter of buried pipe as well as propagation velocity is considered.

3.2.1 Relation between Diameter of Buried Pipe and Image Shift along t-axis

The reflection from a point reflector at depth d

shapes a hyperbola in the x-t radar image as

$$t = \frac{1}{v}\sqrt{x^2 + d^2} \qquad (6)$$

where v is a propagation velocity between the point reflector and the ground surface. Also the shape of reflection from a buried pipe with diameter D is described as

$$t = \frac{1}{v}\sqrt{x^2 + (d + D/2)^2} - \frac{1}{v}D/2 \qquad (7)$$

In the x-t radar image, this curve shows a hyperbola shifted upward by $D/2v$ along t-axis (Fig. 8). In other words, if the radar image is shifted downward by $D/2v$, the reflection of the buried pipe shapes a strict hyperbola, shown in Fig. 8. The image shift procedure can be performed easily and be
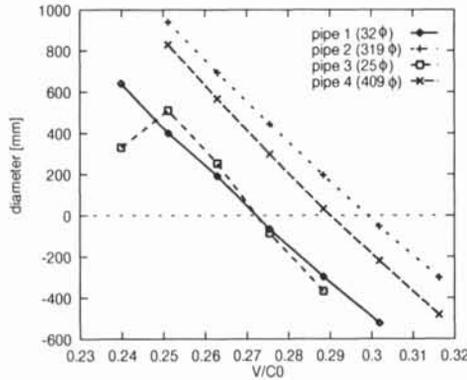
442

Figure 10: Estimated diameters of four pipes. Horizontal axis shows an assumed propagation velocity.

added to the $x-t-v$ method which are assuming that the buried object is a point reflector. In this case, a new axis corresponding to the image shift should be taken in.

3.2.2 Experiments

The estimation of the diameter of buried pipe is experimented using the image shift along t-axis. First, the radar image is shifted along t-axis, and this shifted image is migrated for various propagation velocities. Then, the intensity peak of migrated image is detected on shift-axis for each propagation velocity. This shift value gives an estimate of the diameter of buried pipe.

Concerning the image shown in Fig. 7 the relation between the image shift and the intensity of migrated image are obtained. In Fig. 9 a result of pipe 2 is shown. An intensity peak appears on shift-axis for each propagation velocity. The estimate of diameter for each propagation velocity is calculated by the shift value, at which the intensity has a peak, and each propagation velocity. The estimated diameter of four pipes is shown in Fig. 10. Fig. 10 shows that the estimated diameters separates into two groups which have a difference $400 \sim 500$ [mm]. Two groups correspond to thin pipes (pipe 1, pipe 3) and thick ones (pipe 2, pipe 4) if the propagation velocities of four pipes are equal.

This result shows the relative diameters between thin pipes and thick ones can be estimated using the image shift method. In Fig. 9, the peak intensity for each propagation velocity is slightly decreasing as the image shift increases. Since the image shift procedure makes the reflector deeper, the peak value of migrated image is affected. This effect should be corrected, and the result will be improved.

4 Conclusion

We propose the $x-t-v$ data matrix method for radar imaging of underground pipes in inhomoge-

neous soil without *a priori* knowledge of electromagnetic wave propagation velocity. In the experiment, the effectiveness of our method is demonstrated by comparison with previous methods. Our method assumes that the pipe diameter is negligible to its depth from the ground surface. The influence of thick buried pipes is considered, and the possibility of relative diameter estimation between thin pipes and thick ones is shown, by using the migration method. The pipe diameter will in future be added to the $x-t-v$ data matrix as a parameter, as in the eccentricity-migration method.

References

[1] Tsuchihashi H., Satoh K., Matsuura T., Noguchi H., Uekubo Y. and Usami T., 1989. A new radar system for underground pipes detection. Proc. 10th IEE CIRED'89, pp.247-251.

[2] Osumi N. and Ueno K., 1985. Microwave holographic imaging of underground objects. IEEE Trans. Antennas Propagat., AP-33, pp.152-159.

[3] Stolte C. and Nick K.-P., 1994. Eccentricity-Migration: a method to improve the imaging of pipes in radar reflection data. Proc. 5th International Conference on Ground Penetrating Radar, pp.723-733.

[4] Stolt R. H., 1978. Migration by Fourier transform. Geophysics, 43, pp.23-48.

[5] Ho G. S. and Kawanaka A., 1995. Migration method for subsurface radar considering variation of propagation velocity in depth direction. IEICE Trans. Comm., J78-B-II, pp.638-645.